Sub-cloud turbulence explains cloud-base updrafts for shallow cumulus ensembles: First observational evidence

Youtong Zheng[1], Daniel Rosenfeld[2], and Zhanqing Li[1]

Affiliations:

[1]Earth System Science Interdisciplinary Center, University of Maryland, College Park, Maryland, 20742, USA.

[2]Institute of Earth Science, Hebrew University of Jerusalem, Jerusalem, Israel.

Corresponding author: Youtong Zheng, Earth System Science Interdisciplinary Center, University of Maryland, College Park, Maryland, 20742, USA, zhengyoutong@gmail.com

Key points:

- Doppler lidar observations show sub-cloud turbulence explains half of the variability in cloud-base updrafts for shallow cumulus ensembles
- The relationship has weak diurnal variation except in the early morning and late afternoon
- We develop a new approach of observing ensemble-averaged quantities from lidar measurements made at a fixed point

Abstract

Sub-cloud turbulent kinetic energy has been used to parameterize the cloud-base updraft velocity (w_b) in cumulus parameterizations. The validity of this idea has never been proved in observations. Instead, it was challenged by recent Doppler lidar observations showing a poor correlation between the two. We argue that the low correlation is likely caused by the difficulty of a fixed-point lidar to measure ensemble properties of cumulus fields. Taking advantage of the stationarity and ergodicity of early-afternoon convection, we developed a lidar sampling methodology to measure w_b of a shallow cumulus (ShCu) ensemble (not a single ShCu). By analyzing 128 ShCu ensembles over the Southern Great Plains, we show that the ensemble properties of sub-cloud turbulence explain nearly half of the variability in ensemble-mean w_b, demonstrating the ability of sub-cloud turbulence to dictate w_b. The derived empirical formulas will be useful for developing cumulus parameterizations and satellite inference of w_b.

1. Introduction

Cloud-base updraft velocity (w_b) is a crucially important variable as it influences various aspects of cumulus clouds (Rogers and Yau, 1996). The w_b modulates the aerosol cloud-mediated effect by governing the supersaturation near cloud bases (Twomey, 1959; Rosenfeld, 2014). In polluted conditions, cloud droplet size and number concentration are more sensitive to w_b than aerosol concentration and size (Reutter et al., 2009). Moreover, w_b dictates lateral entrainment of cumulus that remains an unresolved bottleneck for climate modeling (Donner et al., 2016).

Despite its importance, current cumulus parameterization schemes rarely express w_b explicitly (Donner et al., 2016). Most schemes parameterize the cloud-base mass flux (M_b) without specifying the w_b. For example, Arakawa and Schubert (1974) determine the M_b by adjusting the cloud work function towards a value maintaining an equilibrium between the large-scale forcing and the convection. Krishnamurti et al. (1983) determine M_b under the assumption that convection must balance the column integrated vertical advection of moisture. Kain and Fritsch (1993) and Grell (1993) parameterize M_b by requesting the convection to remove the large-scale instability over the convective time scale.

The earliest effort that explicitly represents the w_b in M_b closure is Brown (1979) who approximates the w_b using the environmental vertical velocity from the surrounding nine points at lower tropospheric levels. This scheme is physically flawed by the fact that the air masses that initiate cumulus clouds are convective in nature. This issue is addressed by Neggers et al. (2009) and Fletcher and Bretherton (2010) (FB10) who argued that the w_b could be dictated by the sub-cloud turbulent intensity. FB10 used a set of cloud-resolving simulations to empirically derive the following formula to represent the w_b:

$$w_b = 0.28 \times \mathrm{TKE_{ML}}^{1/2} + 0.64, \qquad (1)$$

in which the $\mathrm{TKE_{ML}}$ is the turbulent kinetic energy averaged horizontally and vertically in the sub-cloud mixed layer. FB10 shows that such a boundary-layer-based mass flux closure scheme outperforms several commonly used schemes for three cumulus cases.

Still lacking is observational evidence of the ability of $\mathrm{TKE_{ML}}$ to explain the w_b. As quoted by Donner et al. (2016): "*... parameterizations that do provide vertical velocities have been*

subject to limited evaluation against what have until recently been scant observations." The only observational pursuit to evaluate the Eq. (1) is from Lareau et al. (2018) who analyzed Doppler lidar observations of ~1500 individual shallow cumulus (ShCu) over the Southern Great Plains (SGP), finding that sub-cloud vertical velocity variance (a proxy for TKE_{ML}) explains only a few percent of the w_b variability. This led them to cast doubt upon the relationship. They argue that sub-cloud updrafts must work against negative buoyancy near the top of the mixed layer to generate w_b, and such a penetrative nature of the convection deteriorates their correlations.

Given the contrasting results, it is imperative to answer the question of whether or not sub-cloud turbulence explains the w_b. This is not only important for cumulus parameterizations but also crucial for advancing other pursuits in the field of cumulus dynamics. First, theoretical inquiries of cumulus dynamics often rely on the assumption of a tight coupling between the sub-cloud turbulence and w_b. For example, in one-dimensional bulk models of boundary layer clouds, a key variable is the Deardoff velocity scale, w^*, which dictates the sub-cloud turbulence intensity (Betts, 1973; Neggers et al., 2006; Stevens, 2006; Zheng, 2019). Linking the w^* with the w_b is the basis for several important coupling processes between the cloud and sub-cloud layers (Neggers et al., 2006; van Stratum et al., 2014; Zheng et al., 2020). Second, recently emerging new satellite remote sensing methodologies of retrieving w_b (Zheng and Rosenfeld, 2015; Zheng et al., 2015, 2016) have offered great insights into the aerosol indirect effect and climate change (Rosenfeld et al., 2016; Seinfeld et al., 2016; Li et al., 2017; Grosvenor et al., 2018; Rosenfeld et al., 2019). These studies infer the w_b via quantifying the TKE_{ML} or its equivalents. Evaluating if the TKE_{ML} explains the w_b is essential to evaluate the physical validity of these techniques.

To that end, this study examines the relationship between the w_b and sub-cloud turbulence for ShCu using DL observations over the SGP. We focus on w_b of ShCu ensembles, not single ShCu, because the former is more relevant to cumulus parameterization. We show that ensemble-averaged w_b and sub-cloud turbulence are highly correlated with statistical significance (correlation coefficient greater than 0.7). Evaluating the relationship on ensembles but not on individual ShCu might explain the disparities with the previous finding (Lareau et al., 2018). The next session discusses the difference between the ensemble-mean w_b and the w_b of single cumuli. It lays the foundation for developing the sampling strategy of ShCu ensembles. Section 3

introduces the observational data and methodology. Section 4 shows the results, followed by a summary.

2. w_b of cumulus ensembles

Distinguishing between the ensemble and individual ShCu is necessary. The concept of cumulus ensemble is a fundamental building block for all cumulus parameterizations (Arakawa and Schubert, 1974). A cumulus ensemble on spatial scales of several tens of kilometers is composed of individual cumulus with a wide range of distributions in size and age. Since the individual cumulus clouds are at different stages of their lifetime, their physical properties differ considerably even if the surface and large-scale forcing are uniform.

The difference could be illustrated by Figure 1 showing a ShCu ensemble simulated by the Weather Research and Forecasting (WRF) in the Large-Eddy Simulation (LES) Atmospheric Radiation Measurements (ARM) Symbiotic Simulation and Observation (LASSO) project (Text S1). The surface fluxes and large-scale forcing are uniform over the 14.4 × 14.4 km domain with a horizontal grid size of 100 m. The vertical velocity field at the cloud-base level shows a distinctive pattern with strong updrafts within clouds surrounding by shells of downdrafts (Fig. 1a). We can see a rough correspondence between the vertical velocity field at the cloud-base level (Fig. 1a) and the TKE_{ML} (Fig. 1b): regions with larger TKE_{ML} typically have stronger updrafts near cloud bases. Such a correspondence, however, breaks down on the length scale of a single ShCu. For example, the vertical velocity field shows strong updrafts within individual clouds surrounding by shells of downdrafts whereas the TKE_{ML} variability across the cloud edges is considerably more uniform. This is not surprising since both updrafts and downdrafts contribute to the vertical mixing, jointly regulating the TKE_{ML}. As a result, their covariation on the length scale of individual ShCu tends to be noisy, which is confirmed by Figure 1c that compares the two quantities averaged over individual ShCu. The degree of scattering is likely to increase substantially when the synoptic and surface forcings are allowed to change.

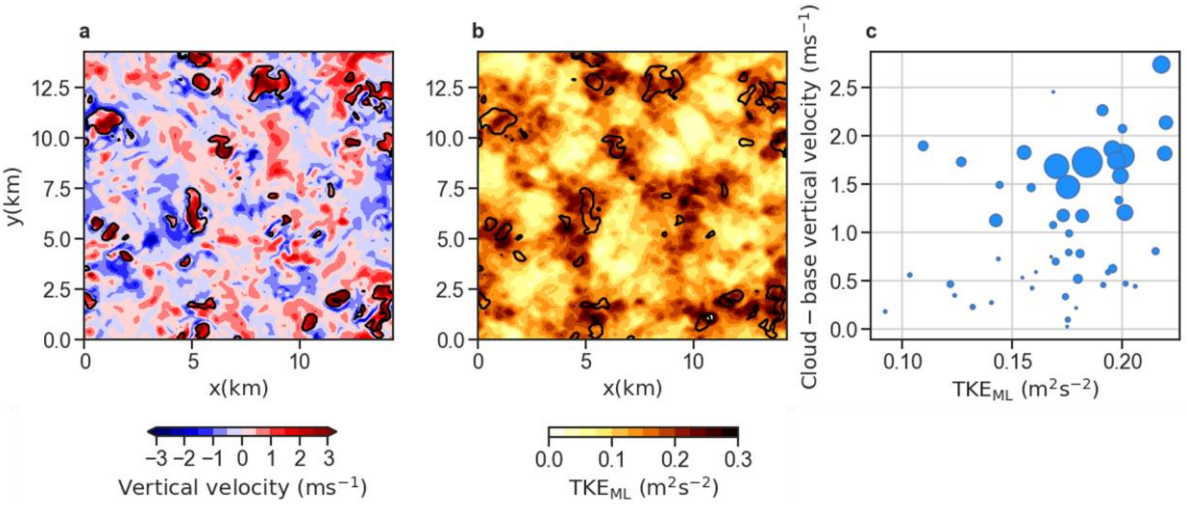

Figure 1: Examples of the different length scales of spatial variability of w_b and TKE_{ML} using WRF-simulated ShCu on 21 UTC, June 6, 2015. (a) Spatial distribution of vertical velocity at the cloud-base level with maximum cloud coverage. Black contours mark the cloudy regions with liquid water content greater than 0.01 g/m^3. (b) The same scene but the color shading is the TKE_{ML}. (c) Scatter plot of cloud-base vertical velocity versus TKE_{ML}, with each point representing mean over individual cumuli. The size of a point is proportional to the size of cumuli. The data are obtained from the first phase of LASSO project. The TKE_{ML} is computed as $0.5(u'^2 + v'^2 + w'^2)$ averaged below the cloud base.

Measuring the ensemble-mean w_b from a surface-based DL, however, is challenging. The DL at a fixed location samples a line of cloud elements along the direction of horizontal winds. In order to sample an adequate amount of individual cumuli to constitute an ensemble, the sampling time window must be at least several hours. For example, for the wind speed of 5 m/s, a 2-hour sampling window corresponds to a distance of ~ 36 km, comparable to the spatial scale of a continental ShCu ensemble. However, ShCu experiences distinctive diurnal variations over the continent. Within the 2-hour sampling period, the ShCu ensemble may evolve, leading to sampling uncertainties. Fortunately, a convective boundary layer often experiences a quasi-steady state (Moeng, 1984; Lensky and Rosenfeld, 2006; Stull, 2012). In atmospheric science, whether a dynamical system can be considered quasi-steady depends on the difference between the

characteristic time scale of the system and the time scale of external forcing. For a typical convective boundary layer over the continent, the surface forcing time scale is on the order of a few hours (defined as half of the period when the surface heat fluxes remain positive) whereas the time scale for shallow convective circulations is several tens of minutes (i.e. the convective time scale) (Fig. S1a). Such a time scale separation allows the mixed layer to remain in a quasi-steady state in which changes in turbulent properties are negligible compared with the turbulence production and dissipation terms (Stull, 2012). This quasi-steady assumption is particularly valid in the early afternoon when the surface fluxes reach their plateau and their time derivatives minimize (Fig. S1b). As such, focusing on early-afternoon ShCu can reduce the uncertainty of sampling due to temporal evolution.

In summary, to measure the w_b of ShCu ensembles from surface-mounted DL, the sampling window must be at least a few hours to sample enough amount of individual ShCu. Moreover, an ideal sampling period is the early afternoon when the boundary layer is close to stationarity.

3. Data and Methodology

We use observations from the Department of Energy's Atmospheric Radiation Measurements (ARM) SGP observatory. The key instrument used in this study is the DL. The DL measures vertical velocity with ~ 1 s temporal and 30 m vertical resolution. The transmitted wavelength is 1.5 μm. In addition to DL, we also use data from radiosondes, a ceilometer, a Ka-band cloud radar (KAZR), and ARM instruments measuring surface meteorological variables routinely.

3.1. An example case

To illustrate the sampling principle of ShCu ensembles, Figure 2a shows a MODIS satellite imagery of a ShCu field over the SGP at 20:30 UTC on June 10, 2012. The wind is southeasterly at a speed of ~ 9 m/s, corresponding to a horizontal distance of ~ 70 km over the two hours (the red solid line in Fig. 2a). One can see a few dozens of single cumuli drifting over the SGP site along the wind direction. Figure 2b shows a time-height plot of the DL from 19 to 21 UTC, corresponding to 13 ~ 15 local standard time (LST). Black dots mark the cloud-base heights (z_b)

183 measured by the ceilometer. To count how many individual cumuli are sampled during this period,
184 we use the DL reflectivity to identify single cumuli. Figure 2c shows the zoomed-in window near
185 cloud bases during the 19:48 ~ 20:00 UTC. The navy contours encompass pixels with DL
186 reflectivity greater than $10^{-4.6}$ m^{-1} sr^{-1}, a threshold that defines cloudy pixels (Lareau et al., 2018).
187 Based on the reflectivity threshold, a total of 84 individual clouds are identified during the 2-h
188 period. The majority of them have a duration shorter than 4 s, which seems too short to constitute
189 a single cloud. Thus, we congregate clouds with gaps < 20 s, reducing the cloud population to 29,
190 with 12 of them lasting longer than 30 s.

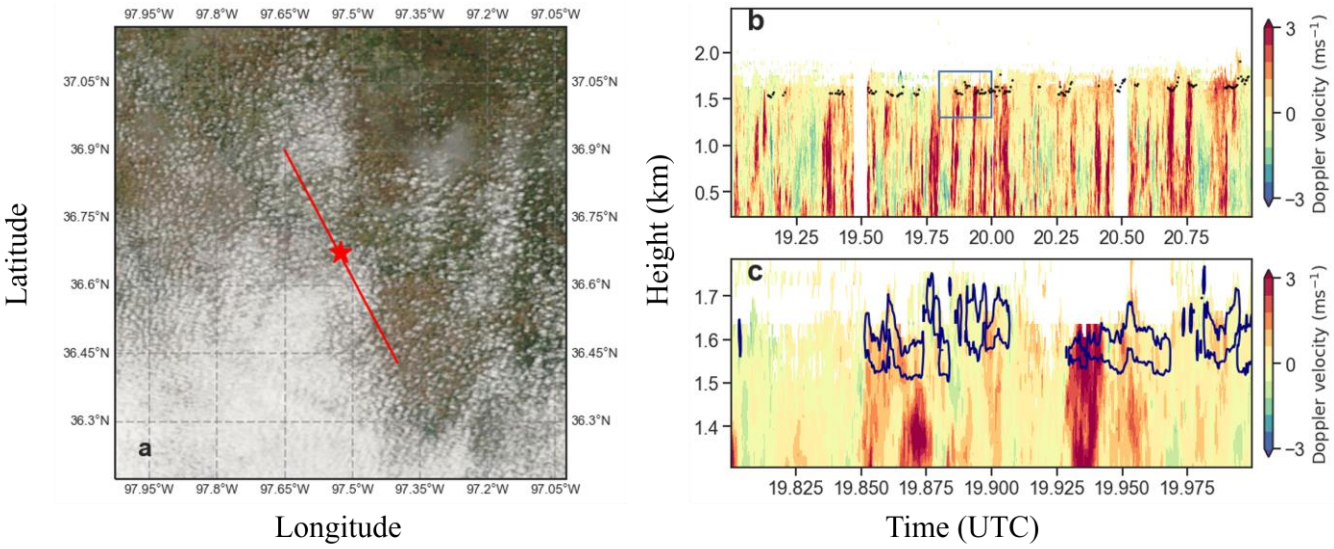

191

192 **Figure 2:** An example case of the shallow cumulus field on Jun 10, 2012, over the SGP.
193 (a) MODIS image centered on the SGP site (red star) at ~20:30 UTC. The red solid line
194 marks the rough direction and travel distance of the mean horizontal wind during the 19 ~
195 21 UTC. (b) Height-time plot of Doppler lidar image of vertical velocity during a two-
196 hour window from 19 to 21 UTC. The black dots mark the cloud-base heights measured
197 by a ceilometer. The blue rectangle marks a smaller window shown in the (c). Navy
198 contours mark the cloudy regions defined as groups of pixels with reflectivity greater
199 than $10^{-4.6}$ m^{-1} sr^{-1}.

200

201

3.2. Computing the w_b

We select "cloud-base" DL pixels through two steps. First, to exclude the decoupled cloud elements and elevated cloud sides, pixels with cloud bases higher than 30% of lifting condensation level (LCL) are removed. Second, for the remaining coupled clouds, we select pixels within three gates below the cloud base (~ 100 m) and cloudy pixels above the cloud base. These pixels are defined as "cloud-base" pixels. Because of the strong signal attenuation, the DL only penetrates < 100 m into the clouds. Therefore, the cloudy pixels are mostly concentrated near several tens of meters above the cloud base. Figure S2 shows a comparison of the vertical velocity probability density function (PDF) between the two sub-groups of "cloud-base" pixels. Their PDF distributions are overall similar, suggesting that it is tenable to combine them as "cloud-base" pixels.

To compute the ensemble-mean w_b, we average the selected vertical velocities in two ways. The first is to simply average the vertical velocities above a threshold: $\overline{w} = \sum N_i w_i / \sum N_i$, in which the N_i represents the frequency of occurrence of positive vertical velocity w_i that is greater than a critical value (w_{crit}). This is the common way for cloud-base mass fluxes study. The second way of averaging is weighted by volume: $\overline{w}^{\mathrm{vol}} = \sum N_i w_i^2 / \sum N_i w_i$. The volume-averaged updraft speed has been considered as more relevant to the understanding of aerosol cloud-mediated effects because it gives more weight to the larger vertical velocities that generate clouds with greater volume (Rosenfeld et al., 2014; Zheng et al., 2015; Rosenfeld et al., 2016).

3.3. Other quantities

Ideally, the $\mathrm{TKE_{ML}}$ should be computed as $0.5(u'^2 + v'^2 + w'^2)$ averaged below the cloud base. However, the DL can only measure the vertical component, $0.5w'^2$, denoted as $\mathrm{TKE^w_{ML}}$. In this study, we use the $\mathrm{TKE^w_{ML}}$ to approximate the $\mathrm{TKE_{ML}}$, motivated by the fact that $\mathrm{TKE^w_{ML}}$ dominates the $\mathrm{TKE_{ML}}$ in typical convective boundary layers (Stull, 2012). The potential contributions from horizontal components of $\mathrm{TKE_{ML}}$ will be taken into account in our analyses in section 3.

We used the surface-measured temperature and moisture to compute the LCL using the exact analytical formula of Romps (2014). As described in the example case, we used the threshold of

DL reflectivity to identify single cumuli. To compute the chord length of individual cumuli, we used the DL product of horizontal wind speed near cloud-base, which is derived from a velocity azimuth display algorithm (Teschke and Lehmann, 2017). The multiplication of cloud-base horizontal wind speed and cloud duration yields the cloud chord length.

3.4. Case selection

A total of 128 ShCu days were selected between 2011 ~ 2014. The selection criterion is in principle similar to previous studies (Zhang and Klein, 2013; Lareau et al., 2018), which involves both objective and subjective criteria. The objective criteria include three steps: (1) the cloud-base height (defined as the mean of the lowest quartile within the 2-h period) has to be within 30% of LCL to ensure coupling, (2) the KAZR reflectivity cannot exceed 0 dBZ between the surface and cloud base to ensure no considerable precipitation, and (3) the cloud duration cannot exceed 30 min to exclude stratiform clouds. Besides, we examine KAZR imageries to ensure ShCu-like characteristics. This is the best we can do since a completely objective method for selecting ShCu remains missing, although the emerging new technique of machine learning is promising to address this issue in the near future (Rasp et al., 2019).

Based on these criteria, we obtain 32 ShCu days per year, similar to the 28 ShCu days per year in Zhang and Klein (2013) and Lareau et al. (2018), suggesting that there is no marked sampling difference between this study and previous ones. Fig S3 shows the statistics of these selected ShCu ensembles. On average, each ensemble is composed of ~ 20 individual ShCu, with half lasting longer than 30 secs. The majority of the ensembles have the maximum cloud chord length shorter than 5 km, consistent with prior knowledge.

4. Results

4.1. Sub-cloud turbulence explains cloud-base updrafts

Figure 3 shows the scatter plots of $\overline{w_b}$ (a) and $\overline{w_b^{vol}}$ (b) versus $(\mathrm{TKE}^{\mathrm{w}}_{\mathrm{M}})^{1/2}$ for different w_{crit}. Overall, the $(\mathrm{TKE}^{\mathrm{w}}_{\mathrm{M}})^{1/2}$ is a good predictor of cloud-base updrafts, explaining ~ 50% of their variabilities. Note that the degree of scattering is still noticeable, but given the instrument error of the DL (~ 0.1 m/s) and potential sampling errors due to the assumption of stationarity, such degrees

of correlation are good enough for demonstrating the physical validness. To our knowledge, this is the first observational evidence supporting the ability of the sub-cloud turbulence to dictate cloud-base updrafts that was only found in high-resolution models (Grant and Brown, 1999; Fletcher and Bretherton, 2010; van Stratum et al., 2014). Such good correlations suggest a continuity of vertical momentum between the sub-cloud layer and cloud base, despite the in-between weakly stable layer (i.e. cloud-base transition layer) (Neggers et al., 2007; Stevens, 2007). Indeed, the stability of the transition layer interacts with the convective circulation, a manifestation of the dynamical coupling between the sub-cloud and cloud layers, to reach an equilibrium that maintains the mass conservation (Neggers et al., 2006; Fletcher and Bretherton, 2010). In this regard, the transition layer property should not be considered an external forcing that alters the coupling between the sub-cloud and cloud-base dynamics, but an internal parameter that responds to the circulation.

Both $\overline{w_b}$ and $\overline{w_b^{vol}}$ increase with the w_{crit}, but the $\overline{w_b^{vol}}$ shows much weaker sensitivity primarily because the $\overline{w_b^{vol}}$ gives more weight to the larger vertical velocities. The intercepts also increase with w_{crit}, which is an artificial consequence of using non-zero w_{crit}. Physically speaking, a zero TKE^{w}_{M} should lead to zero cloud-base updraft speed. Therefore, we will focus our subsequent discussions on the slopes that bear more physical meaning than intercepts.

To compare our results with that from FB10, we visualize the Eq. (1) in Figure 3a (light blue curve). FB10 uses the w_{crit} of 0.5 m/s. Our empirical estimate (the red line) shows a stronger sensitivity of $\overline{w_b}$ to the sub-cloud turbulence than FB10 by more than a factor of 3. What causes the difference? One possible reason is that we used the TKE^{w}_{M} that does not include the horizontal components of the TKE, leading to smaller values of TKE and, thus, a steeper slope. Another more likely reason is that the horizontal resolutions of the model used by FB10 are too coarse (1 km) to accurately simulate the vertical velocities. For instance, modeled vertical velocities decrease with the model resolution by a power law of -2/3 (Rauscher et al., 2016; Donner et al., 2016). The underestimated $\overline{w_b}$ due to low resolution may flatten the slope of $\overline{w_b}$ versus $(TKE_{ML})^{1/2}$ in FB10.

To understand which factor is responsible, we use the LES data of 18 ShCu days from the LASSO project (Text S1). The LASSO horizontal resolution is 100 m, 10 times finer than that used in FB10. With the model output of three-dimensional winds, we are able to diagnose the full

components of TKE_{ML} so that we can conduct an "apple-to-apple" comparison between the LASSO and FB10. As shown by the green lines in Fig. 3a, LASSO models (WRF and System for Atmospheric Modeling, SAM) show slopes steeper than the FB10 by more than a factor of 3 (see Fig. S4 for their scatter plots with statistical details). This confirms that the flatter slope of FB10 is likely caused by the coarse model resolution. The comparison between the LASSO and DL, which is not the focus of this study, is discussed in the supplementary material (Text S2).

We have tabulated the empirical formulas for $\overline{w_b}$ and $\overline{w_b^{vol}}$ for different w_{crit} (Table S1) so that readers can use what suits their research interests.

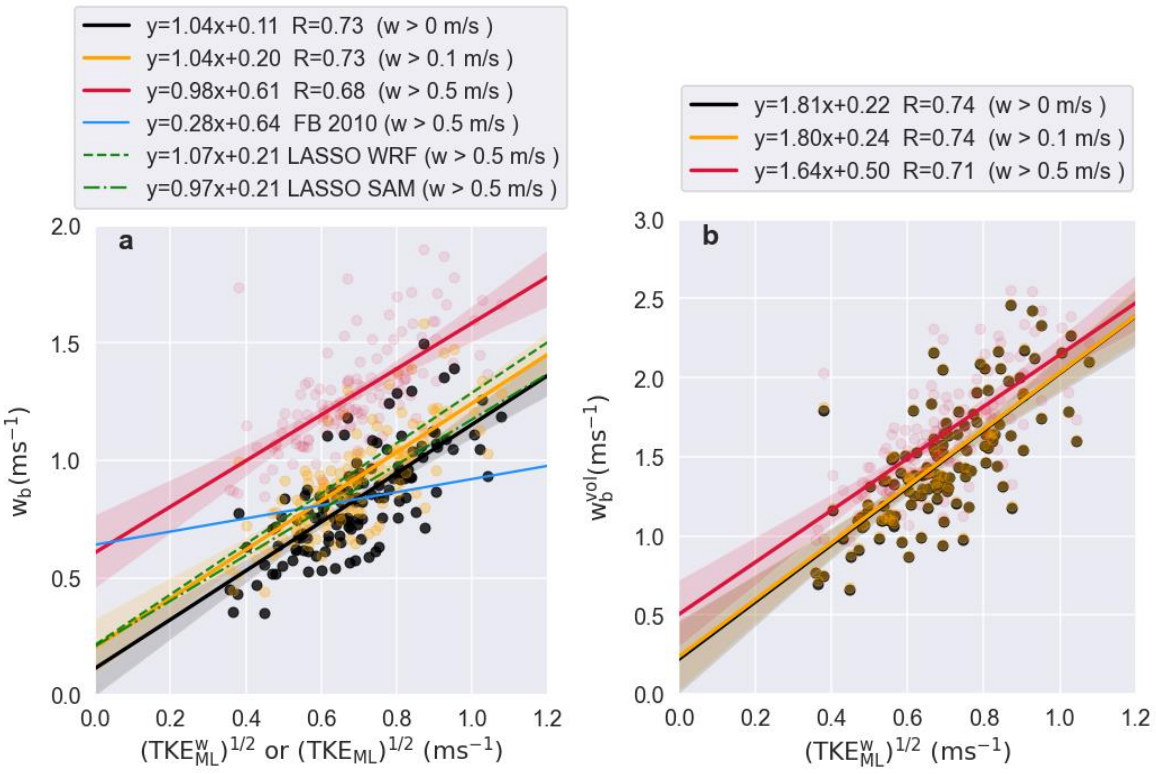

Figure 3: Scatter plots of $\overline{w_b}$ (a) and $\overline{w_b^{vol}}$ (b) versus $(TKE^w_M)^{1/2}$ for w_{cri} = 0, 0.1, and 0.5 m/s. Each point represents a ShCu ensemble mean. The blue solid line marks the Eq. (1), the empirical formula developed in Fletcher and Bretherton (2010).

4.2.Diurnal dependence

Given that all cases are in the early afternoon, one may ask how the observed relationship is representative of the other times of a diurnal cycle. To address this question, we use the LAASO data to examine its diurnal dependence. We chose the w_{crit} = 0 m/s for determining the $\overline{w_b}$ because, as noted above, using an ad-hoc w_{crit}, say 0.5 m/s, leads to a markedly positive $\overline{w_b}$ for zero $(TKE^{w}_{M})^{1/2}$. By using w_{cri} = 0 m/s, we can force the best-fit line through the origin through the least-square algorithm, freeing us from the unphysical meaning of positive intercepts. Figure 4a and b show the scatterplots of the $\overline{w_b}$ versus $(TKE^{w}_{M})^{1/2}$ in different local times simulated by WRF and SAM, respectively. Both models show notably significant correlations between the two quantities in different phases of a diurnal cycle, confirming the ability of $(TKE^{w}_{M})^{1/2}$ to explain the variability of $\overline{w_b}$. More importantly, the slope of the relationship varies little with local time, except in the early morning and late afternoon (Fig. 4c and d). In the early morning, the stronger capping inversion weakens the speeds of rising thermals when they penetrating into the inversion, leading to smaller $\overline{w_b}$ for given sub-cloud turbulence (Fig. S1c). Such a stabilization effect becomes less influential as the convection kicks up, which lessens the inversion strength. In the late afternoon, as the solar insolation weakens, the surface fluxes decrease considerably whereas the boundary layer remains deep (Fig. S1d). This leads to a decoupling between the ShCu and the surface (Stull, 2012), which may explain the flatter slope between $\overline{w_b}$ and $(TKE^{w}_{M})^{1/2}$ in the late afternoon.

In summary, the diurnal dependence of the coupling between the w_b and sub-cloud turbulence is small, except in the early morning and late afternoon when the strong capping inversion and cloud-surface decoupling may lead to flatter slopes, respectively.

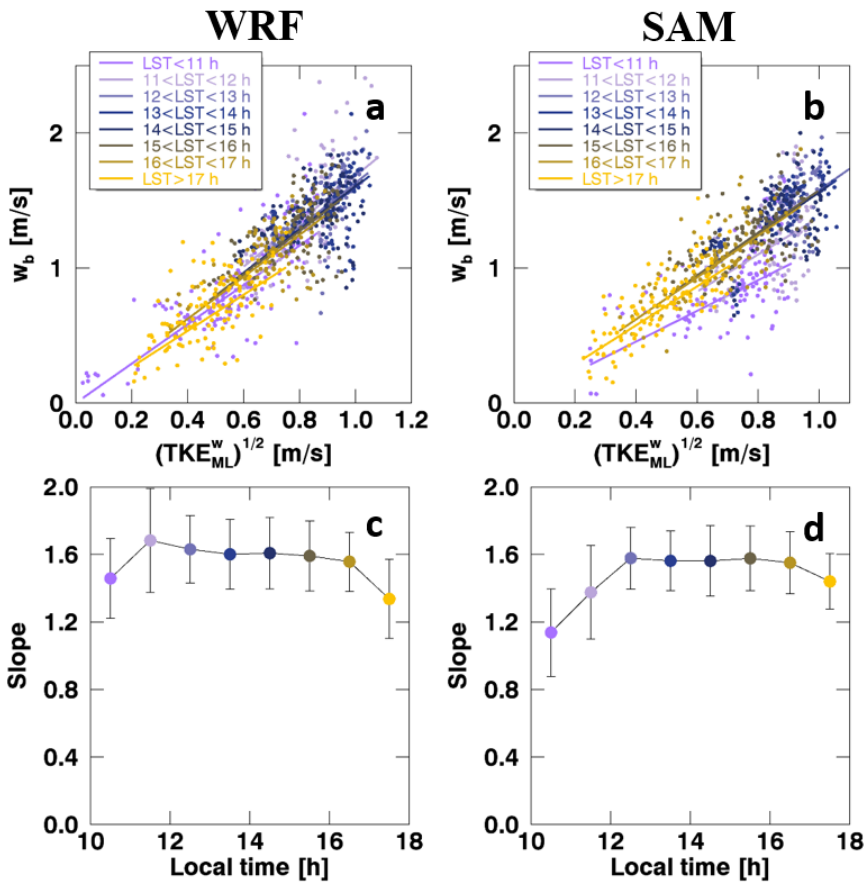

Figure 4: Scatterplots of $\overline{w_b}$ (w_{crit} = 0 m/s) versus the $(TKE^w_M)^{1/2}$ grouped by the local standard time, simulated by WRF (a) and SAM (b). Each group of points corresponds to a best-fit linear regression line forced through zero. The slopes of the best-fit lines are plotted in (c) and (d) for WRF and SAM, respectively.

5. Conclusion

This study examines the relationship between the sub-cloud turbulence and cloud base updrafts using Doppler lidar (DL) observations of 128 shallow cumulus (ShCu) ensembles over the Southern Great Plains. We proposed a new DL sampling method that allows measuring the cloud-base updrafts for an ensemble, instead of individual, ShCu. Specifically, we take advantage of the stationarity and ergodicity of ShCu-topped boundary layers in the early afternoon when the temporal change in the surface forcing is minimum. For each ShCu case, we selected a 2-hour window of DL that includes an average amount of ~ 20 individual cumuli with varying sizes, constituting an ensemble. This allows us to compute the ensemble-averaged quantities from DL

measurements made at a fixed point. By analyzing the 128 ShCu ensembles, we found that the vertical velocity variance explains ~ 50% variability of ensemble-mean cloud-base updrafts, thus supporting the widely-held hypothesis and practice of using the sub-cloud turbulent kinetic energy to parameterize the cloud-base updrafts in some state-of-the-art mass flux closure schemes of convection parameterization (Bretherton et al., 2004; Neggers et al., 2009; Fletcher and Bretherton, 2010). To our knowledge, this is the first observational evidence that demonstrates the ability of sub-cloud turbulence intensity to dictate the cloud-base updrafts.

With the observational data, we derived empirical relationships between the square-root of sub-cloud turbulent kinetic energy and ensemble-mean cloud-base updraft speeds that are computed for different thresholds of vertical velocity and by different averaging schemes. Although all the 128 cases were sampled in the early afternoon, the diurnal variation of the relationship is weak (except in the early morning and late afternoon), as shown by the LES simulations of 18 ShCu cases over the SGP. These empirical formulas are useful for the developments of cumulus parameterizations, theoretical studies of ShCu dynamics, and satellite-based inference of cloud-base updrafts.

Acknowledgments

This study is supported by the Department of Energy (DOE) Atmospheric System Research program (DE-SC0018996). The ground-based data in this study are available from the website of ARM Climate Research Facility (www.archive.arm.gov/data). The LASSO data are available from www.archive.arm.gov/lassobrowser. We thank the LASSO staff for maintaining the data in a user-friendly way.

References:

Arakawa, A., & Schubert, W. H. (1974). Interaction of a cumulus cloud ensemble with the large-scale environment, Part I. *Journal of the Atmospheric Sciences, 31*(3), 674-701.

Betts, A. (1973). Non-precipitating cumulus convection and its parameterization. *Quarterly Journal of the Royal Meteorological Society, 99*(419), 178-196.

Bretherton, C. S., McCaa, J. R., & Grenier, H. (2004). A new parameterization for shallow cumulus convection and its application to marine subtropical cloud-topped boundary layers. Part I: Description and 1D results. *Monthly Weather Review, 132*(4), 864-882.

Brown, J. M. (1979). Mesoscale unsaturated downdrafts driven by rainfall evaporation: A numerical study. *Journal of the Atmospheric Sciences, 36*(2), 313-338.

Donner, L. J., O'Brien, T. A., Rieger, D., Vogel, B., & Cooke, W. F. (2016). Are atmospheric updrafts a key to unlocking climate forcing and sensitivity? *Atmospheric Chemistry and Physics, 16*(20), 12983-12992. <Go to ISI>://WOS:000386665800002

Fletcher, J. K., & Bretherton, C. S. (2010). Evaluating boundary layer–based mass flux closures using cloud-resolving model simulations of deep convection. *Journal of the Atmospheric Sciences, 67*(7), 2212-2225.

Grant, A., & Brown, A. (1999). A similarity hypothesis for shallow-cumulus transports. *Quarterly Journal of the Royal Meteorological Society, 125*(558), 1913-1936.

Grell, G. A. (1993). Prognostic evaluation of assumptions used by cumulus parameterizations. *Monthly Weather Review, 121*(3), 764-787.

Grosvenor, D. P., Sourdeval, O., Zuidema, P., Ackerman, A., Alexandrov, M. D., Bennartz, R., et al. (2018). Remote sensing of droplet number concentration in warm clouds: A review of the current state of knowledge and perspectives. *Reviews of Geophysics, 56*(2), 409-453.

Kain, J. S., & Fritsch, J. M. (1993). Convective parameterization for mesoscale models: The Kain-Fritsch scheme. In *The representation of cumulus convection in numerical models* (pp. 165-170): Springer.

Krishnamurti, T. N., Low-Nam, S., & Pasch, R. (1983). Cumulus parameterization and rainfall rates II. *Monthly Weather Review, 111*(4), 815-828.

Lareau, N. P., Zhang, Y., & Klein, S. A. (2018). Observed boundary layer controls on shallow cumulus at the ARM Southern Great Plains site. *Journal of the Atmospheric Sciences, 75*(7), 2235-2255.

Lensky, I., & Rosenfeld, D. (2006). The time-space exchangeability of satellite retrieved relations between cloud top temperature and particle effective radius.

Li, Z., Rosenfeld, D., & Fan, J. (2017). *Aerosols and their Impact on Radiation, Clouds, Precipitation & Severe Weather Events*. Retrieved from

Moeng, C.-H. (1984). A large-eddy-simulation model for the study of planetary boundary-layer turbulence. *Journal of the Atmospheric Sciences, 41*(13), 2052-2062.

Neggers, R., Stevens, B., & Neelin, J. (2007). Variance scaling in shallow-cumulus-topped mixed layers. *Quarterly Journal of the Royal Meteorological Society: A journal of the atmospheric sciences, applied meteorology and physical oceanography, 133*(628), 1629-1641.

Neggers, R., Stevens, B., & Neelin, J. D. (2006). A simple equilibrium model for shallow-cumulus-topped mixed layers. *Theoretical and Computational Fluid Dynamics, 20*(5-6), 305-322.

Neggers, R. A., Köhler, M., & Beljaars, A. C. (2009). A dual mass flux framework for boundary layer convection. Part I: Transport. *Journal of the Atmospheric Sciences, 66*(6), 1465-1487.

Rasp, S., Schulz, H., Bony, S., & Stevens, B. (2019). Combining crowd-sourcing and deep learning to explore the meso-scale organization of shallow convection. *arXiv preprint arXiv:1906.01906*.

Reutter, P., Su, H., Trentmann, J., Simmel, M., Rose, D., Gunthe, S., et al. (2009). Aerosol-and updraft-limited regimes of cloud droplet formation: influence of particle number, size and hygroscopicity on the activation of cloud condensation nuclei (CCN). *Atmospheric Chemistry and Physics, 9*(18), 7067-7080.

Rogers, R., & Yau, M. K. (1996). *A short course in cloud physics*: Elsevier.

Romps, D. M. (2014). An analytical model for tropical relative humidity. *Journal of Climate, 27*(19), 7432-7449.

Rosenfeld, D. (2014). Climate effects of aerosol-cloud interactions. *Science, 1247490*(379), 343.

Rosenfeld, D., Fischman, B., Zheng, Y., Goren, T., & Giguzin, D. (2014). Combined satellite and radar retrievals of drop concentration and CCN at convective cloud base. *Geophysical Research Letters, 41*(9), 3259-3265.

Rosenfeld, D., Zheng, Y., Hashimshoni, E., Pöhlker, M. L., Jefferson, A., Pöhlker, C., et al. (2016). Satellite retrieval of cloud condensation nuclei concentrations by using clouds as CCN chambers. *Proceedings of the National Academy of Sciences*, 201514044.

Rosenfeld, D., Zhu, Y., Wang, M., Zheng, Y., Goren, T., & Yu, S. (2019). Aerosol-driven droplet concentrations dominate coverage and water of oceanic low-level clouds. *Science, 363*(6427), eaav0566.

Seinfeld, J. H., Bretherton, C., Carslaw, K. S., Coe, H., DeMott, P. J., Dunlea, E. J., et al. (2016). Improving our fundamental understanding of the role of aerosol− cloud interactions in the climate system. *Proceedings of the National Academy of Sciences, 113*(21), 5781-5790.

Stevens, B. (2006). Bulk boundary-layer concepts for simplified models of tropical dynamics. *Theoretical and Computational Fluid Dynamics, 20*(5-6), 279-304.

Stevens, B. (2007). On the growth of layers of nonprecipitating cumulus convection. *Journal of the Atmospheric Sciences, 64*(8), 2916-2931.

Stull, R. B. (2012). *An introduction to boundary layer meteorology* (Vol. 13): Springer Science & Business Media.

Teschke, G., & Lehmann, V. (2017). Mean wind vector estimation using the velocity–azimuth display (VAD) method: an explicit algebraic solution. *Atmospheric Measurement Techniques, 10*(9), 3265.

Twomey, S. (1959). The nuclei of natural cloud formation part II: The supersaturation in natural clouds and the variation of cloud droplet concentration. *Geofisica pura e applicata, 43*(1), 243-249.

van Stratum, B. J., Vilá-Guerau de Arellano, J., van Heerwaarden, C. C., & Ouwersloot, H. G. (2014). Subcloud-layer feedbacks driven by the mass flux of shallow cumulus convection over land. *Journal of the Atmospheric Sciences, 71*(3), 881-895.

Zhang, Y., & Klein, S. A. (2013). Factors controlling the vertical extent of fair-weather shallow cumulus clouds over land: Investigation of diurnal-cycle observations collected at the ARM Southern Great Plains site. *Journal of the Atmospheric Sciences, 70*(4), 1297-1315.

Zheng, Y. (2019). Theoretical understanding of the linear relationship between convective updrafts and cloud-base height for shallow cumulus clouds. Part I: Maritime conditions. *Journal of the Atmospheric Sciences*(2019).

Zheng, Y., & Rosenfeld, D. (2015). Linear relation between convective cloud base height and updrafts and application to satellite retrievals. *Geophysical Research Letters, 42*(15), 6485-6491. <Go to ISI>://WOS:000360414900044

Zheng, Y., Rosenfeld, D., & Li, Z. (2015). Satellite inference of thermals and cloud-base updraft speeds based on retrieved surface and cloud-base temperatures. *Journal of the Atmospheric Sciences, 72*(6), 2411-2428.

Zheng, Y., Rosenfeld, D., & Li, Z. (2016). Quantifying cloud base updraft speeds of marine stratocumulus from cloud top radiative cooling. *Geophysical Research Letters, 43*(21).

Zheng, Y., Sakradzija, M., Lee, S.-S., & Li, Z. (2020). Theoretical understanding of the linear relationship between convective updrafts and cloud-base height for shallow cumulus clouds. Part II: Continental conditions. *Journal of the Atmospheric Sciences, 77*(4), 1313-1328.